Biophysical Journal, Volume 98

Supporting Material

Force Generation and Dynamics of Individual Cilia under External Loading

David B. Hill, Vinay Swaminathan, Ashley Estes, Jeremy Cribb, E. Timothy O'Brien, C. William Davis, and Richard Superfine

Supplemental Materials

Culture Preparation

Normal Human Bronchial Epithelial cells were cultured on 0.4 micron pore sized millicell membranes (Millipore Corp. USA) coated with collagen and maintained in Air Liquid Interface Media (UNC Tissue Core) as previously described (1). Over a period of 6 weeks, confluent cultures developed cilia. Once well ciliated, cultures were washed twice for 20 minutes in PBS to remove the bulk of the mucus layer. These were next incubated at 37^0C for 30 minutes in 50μM ATP in phosphate buffered saline (PBS) to stimulate cells to release all stored mucins (2). Following the stimulated mucin secretion, cultures were washed twice for 10 minutes in PBS, and then washed for 10 minutes in 10mM dithiothreitol (DTT) in PBS. Following two additional PBS washes to remove all free DTT and remaining mucus, cultures were incubated in a 1/5000 dilution of biotinylated wheatgerm agglutinin (β-WGA) (Vector laboratories Inc., Burlingame, USA) for 15 minutes. Cultures were then washed twice for 10 minutes in PBS and incubated at 4^0C for 30 minutes in <1% v/v streptavidin-coated 2.8μm magnetic beads (Dynal Biotech, Oslo, Norway). To insure binding to a single cilium, the beads were coated with gold except for a single, ~100 nm diameter spot. (described below). Cultures were then washed one final time, and the cell layer(s) and underlying membrane removed from the culture dish and transferred onto number 0 cover slips to be loaded into the 3DFM.

Force Microscopy

The 3DFM applies forces to magnetic beads through the generation of magnetic field gradients via independently addressable multiple electromagnets. Flux is directed through magnetic pole tips arranged in space to provide the necessary directional capability (3-5). The

instrument is combined with a conventional inverted optical microscope (Nikon TE-2000E, 40x/0.60 NA objective with a 1.5x image magnifier), and brightfield image data aquired at 120 frames per second using a Pulnix 8-bit video camera. Beads of interest within the videos were tracked using Video Spot Tracker (developed by The Center for Computer Integrated Systems for Microscopy and Manipulation at The University of North Carolina at Chapel Hill, available at http://www.cs.unc.edu/Research/nano/cismm/download/spottracker/video_spot_tracker.html) using a symmetric tracking kernel, and the "follow jumps" option. The video Spot Tracker takes a model-based approach to tracking spots, where the model of the intensity distribution within the spot is used to find the center of each tracked spot to sub-pixel accuracy. It is robust to image noise that is uncorrelated with the spot cross section. Once tracked, the position data for each bead was analysis using Matlab scripts that find the local minimum and maximums of the bead motion, as well as the instantaneous velocity of the tip. The amplitude of the cilia beat cycle was then calculated from the difference in the average max and min for the bead during both the presence and absence of magnetic force. Frequency analysis was performed by inverting the average period of the cilia beat cycle.

Magnetics Calibration

The force acting on a 2.8 micron magnetic bead was determined as a function of its location and the magnetic drive current. The magnets were driven with a repeated sequence of step pulses of ascending amplitude on a sample containing 2.8 micron beads in 2.5M sucrose. The bead velocity at each position was determined using Video Spot Tracker. The forces applied to each sphere were computed using Stokes' relationship. The resulting force and position information were synchronized with the magnet drive history during an experiment, and

interpolated to determine the force on a bead as a function of location and drive current (Figure S1-B). Only one pole tip was used for our experiments, where the pole tip could be positioned as close as 10 microns from a magnetic bead.

Spot Labeled Beads

To measure single cilium dynamics, it was important to have a single, small functional spot on our magnetic beads to reduce non-specific binding. To make spot labeled beads, 2.8 micron magnetic beads (Dynal/Invitrogen), functionalized with streptavidin were dried on a cover slip and then sputter coated with a thin layer of gold. Due to contact, a small spot on the bead remained uncoated. The beads on the coverslip were then coated with thiol-PEG (Polyethylene glycol) (Nektar Therapeutics, USA) and then released from the coverslip. To test the single spot functionalizing of the beads, small biotinylated targets (200nm fluorescent beads) were added to spot-labeled beads and then imaged. Selective binding on the magnetic bead surface can be clearly seen in Figure S2-D.

Determination of Effective and Recovery Strokes

To differentiate between the effective and recovery strokes of the cilia's beat, we digitized the beat shapes presented by Aiello and Sleigh for frog palate epithelial cilia (6) (Figure S2A). From these shapes, the projection of the tip of the cilium at each time presented by Aiello and Sleigh can be compared to the bead track presented in the present paper (Figure 2C). We note that as the beat enters the effective stroke, the tip velocity is the highest it will be at any point during the beat cycle. During the effective stroke, the cilia begins to slow from it's initial high velocity (or slope as it is presented in Figure S2B) until it enters a "lag" phase, or gradual

transition from the effective to recovery stroke, clearly denoted by the broad peaks seen in Figure S2B. Once the tip begins to travel away from the maximum displacement reached in the effective stroke, the velocity (or slope) is less than during the effective stroke. The transition between the recovery and effective stroke is more rapid than the transition from effective to recovery strokes, and is denoted by the sharp trough seen in Figure S1B. The qualitative similarities in slopes and stroke transitions seen in Figure S2B relative to Figure 2C gives us confidence in our assignment of the effective and recovery strokes.

Stiffness

A singlet microtubule (with outside radius $r_s = 12nm$) has an area moment of inertia I given by $I_{SM} = (\pi/4)r_s^4$. For the elliptical doublet microtubule with semimajor axis $r_a = 20nm$ and semiminor axis $r_b = 12nm$, bending with its neutral plane at an angle θ to the semimajor axis, $I_{dm} = (\pi/4)(I_a \cos^2\theta + I_b \sin^2\theta)$ where $I_a = (\pi/4)r_a^3 r_b$ and $I_b = (\pi/4)r_b^3 r_a$. Using the appropriate angles from the standard axoneme geometry, we have the angles for the microtubule doublets as $\theta = 0, \pm 40, \pm 80, \pm 120, \pm 160$ degrees. If we assume that there are no connecting proteins, the individual terms contribute in a simple additive manner and we calculate that the outer doublets contribute $I_{outerdoublets} = 26.I_{SM}$. If we include the central two singlet microtubules we obtain $I_{axoneme} = 28I_{SM}$ (27).

Motor Force

In this model the elastic rod is composed of two microtubule doublets where the local, relative sliding of the microtubules results in the curvature of the rod. When only the internal

shear forces are imposed, the total energy of the filaments is minimized for a particular curvature $C_0(x) = aF(x)/EI$ (7) where *a* is the spacing between the microtubules, and $F(x) = -\int_x^L f(x')dx'$ is the integral of the internal shear force density *f(x')* from the point of interest to the filament end. Taking the simplest case where the internal shear force density $f(x')=f$ is constant, and the curvature due to internal stresses is added linearly with the curvature due to a point force imposed at the rod end $F_{B,}$ we find the rod curvature given by $d^2y/dx^2 = LF_B\delta(L)/EI + C_0$. By solving the above equation for the displacement of the doublets, and imposing stall at the tip or that y=0 when x=L, we get $F_B = af \equiv F_M$. Thus in terms of the molecular motor force, we find $F_m = a F_{RM}/\delta$ where F_{RM} is motor force per repeat length δ.

Geometry of the Axoneme

To estimate the force contribution of a single active dynein, we use a geometrical argument based on the angles made by the contributing MTs with the bending direction. Figure SM3 (Supporting Materials) is a simple illustration of this geometry, where each contributing dynein column is represented as *A, B, C* and *D.* Thus the effective contribution of the dyneins is given by

$$F_{PM} = F_A \cos 70^\circ + F_B \cos 30^\circ + F_C \cos 10^\circ + F_D \cos 50^\circ$$

Assuming that the force within the columns is equal, this reduces to

$$F_{PM} = 2.84 \cdot F_{SD}$$

F_{PM} is the force per motor domain and from our model is found to be 16pN. Thus the force per active dynein or F_{SD} is 5.6pN.

Fitting Data to Model

We interpret our data through a one dimensional model for the cilium including the bending stiffness of the axoneme, the effects of the internal motor forces and the force of the attached bead. To model the amplitude reduction of the cilium, we model it as a stiffening spring with a non linear term. We assume a quasi static case where the force equilibrium equation is written as

$$F_B + F_m = F_A$$

and F_m and F_A are defined as

$$F_m = f\sin(\omega t)$$

$$F_A = k_A x + k_A' x^3$$

Since our model only captures the end point of the cilia beat cycle under amplitude reductions, we replace the motor force term with an effective motor force f. Substituting the last 2 equations into the first equation, we get a standardized form for our force equilibrium equation given by

$$x^3 + \frac{k_A}{k_A'} x - \left(\frac{F_B + f}{k_A'} \right) = 0$$

The above equation is a standard 3rd order polynomial equation. Solving it for x, we get a solution for x given by:

$$x = \frac{-k_A / k_A'}{3\left[(F_B \pm f)^2 / 2k_A' - \sqrt{(F_B \pm f)^2 / 4k_A'^2 + k_A^3 / 27k_A'^3} \right]^{1/3}} + \left[(F_B \pm f) / 2k_A' - \sqrt{(F_B \pm f)^2 / 4k_A'^2 + k_A^3 / 27k_A'^3} \right]^{1/3}$$

The maximum displacement of the axoneme tip is defined by the case when the applied force is in the same direction as the internal effective motor force ($F_B + f$) and the minimum as the external force acting against the internal force ($F_B - f$). Thus the change in CBA is given by:

$$\delta x = \frac{x_{max} - x_{min}}{\delta x_0}$$

It should be noted that x is a function of F_B as well as the ratio k_A/k_A' and f. Similarly δx has the same dependence as x, but is also dependent on the baseline beat amplitude given by δx_0 in the above equation. The data is fitted to above final equation by allowing k_A, k_A', f and δx_0 to be varied by a least square solver.

Supplementary Figures:

Figure SM1

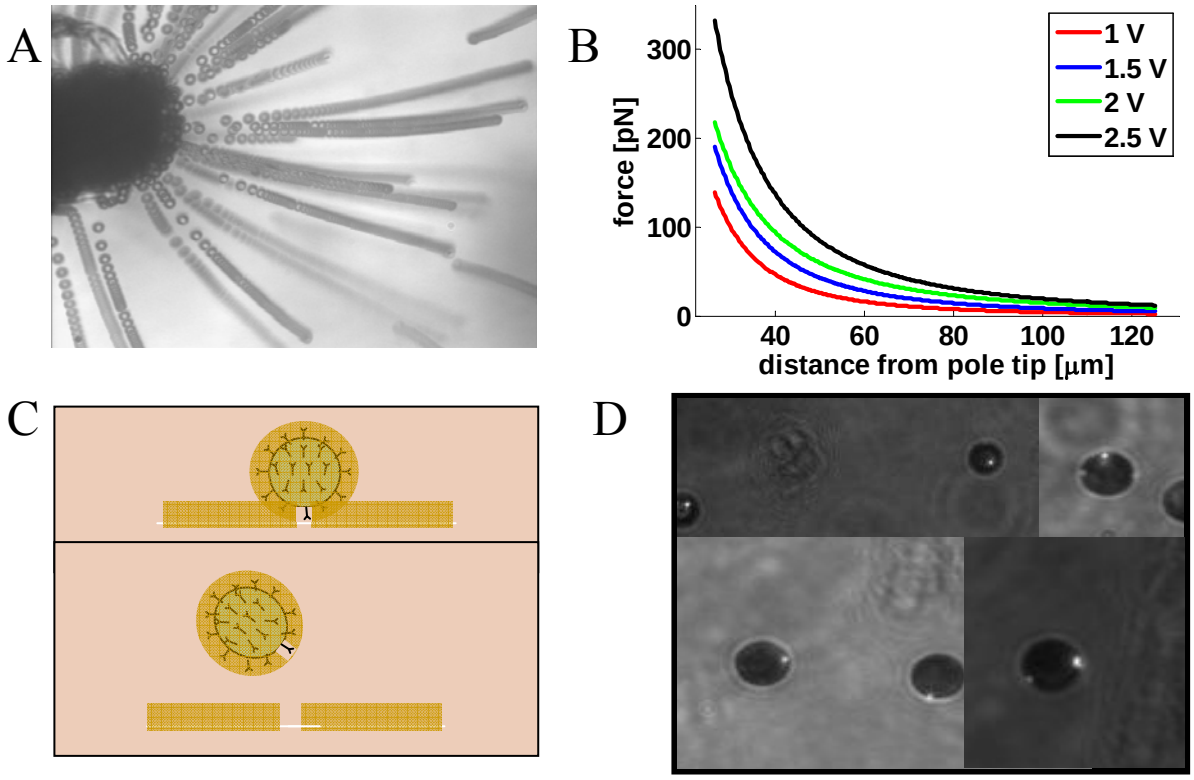

Figure S1 A) Maximum Intensity projection of beads in 2.5M sucrose used for calibration of the pole tip. B) Calibration plot of force vs. distance for 2.8 micron magnetic beads in 2.5M sucrose at different voltages C) Illustration of the spot-labeling process where the bead is first dried on the cover slip and then sputter-coated with a gold layer finally to be released from the cover slip. D) Brightfield and fluorescence images of spot labeled beads that have been mixed with 200 nm biotin labeled fluorescent beads. The small beads bind to a single spot on each individual bead. All beads are 2.8 microns in diameter.

Figure SM-2

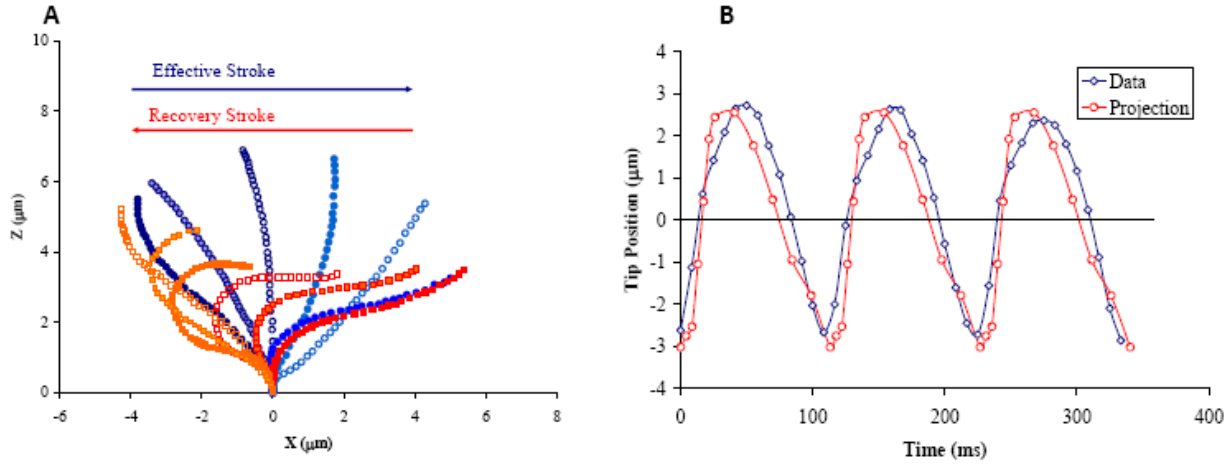

Figure S2: Extrapolating the Effective and Recovery strokes. A) Digitization Figure 2a and b from Aiello and Sleigh (77) beat shapes from frog palate epithelium cilia. B) Comparing the 1-D Project of the tip of the Cilium from Figure S1A to the tracked motion of a bead attached to a cilium (Figure 2Ci). The time stamps for the projected data at 10ms between shapes during the recovery stroke a 3ms between shapes during the effective stroke. The amplitude and frequency of the project data has been evenly adjusted to match that of the tracked bead from Figure 2Ci

Figure SM 3

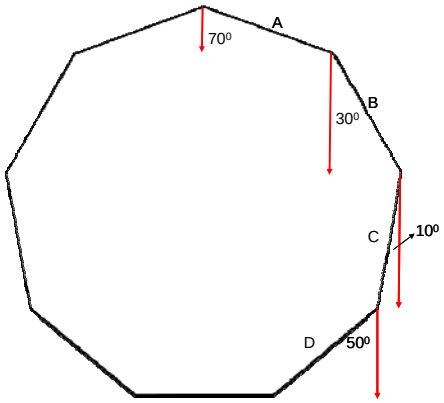

Figure S3- *Schematic of the Axoneme. Segments A, B, C, and D represent columns of active dyneins.*

1. Fulcher, M. L., S. Gabriel, K. A. Burns, J. R. Yankaskas, and S. H. Randell. 2005. Well-differentiated human airway epithelial cell cultures. Methods Mol Med 107:183-206.
2. Davis, C. W., M. L. Dowell, M. Lethem, and M. Vanscott. 1991. Stimulation of Goblet Cell Degranulation by Exogenous Atp in Isolated Canine Tracheal Epithelium. Faseb Journal 5:A1397-a1397.
3. Fisher, J. K., J. Cribb, K. V. Desai, L. Vicci, B. Wilde, K. Keller, R. M. Taylor, J. Haase, K. Bloom, E. T. O'Brien, and R. Superfine. 2006. Thin-foil magnetic force system for high-numerical-aperture microscopy. Rev. Sci. Instrum. 77:-.
4. Fisher, J. K., J. R. Cummings, K. V. Desai, L. Vicci, B. Wilde, K. Keller, C. Weigle, G. Bishop, R. M. Taylor, C. W. Davis, R. C. Boucher, E. T. O'Brien, and R. Superfine. 2005. Three-dimensional force microscope: A nanometric optical tracking and magnetic manipulation system for the biomedical sciences. Rev. Sci. Instrum. 76.
5. O'Brien, E. T., J. Cribb, D. Marshburn, R. M. Taylor, and R. Superfine. 2008. Magnetic Manipulation for Force Measurements in Cell Biology. In Biophysical Tools for Biologists, Vol 2: In Vivo Techniques. Elsevier Academic Press Inc, San Diego. 433-+.
6. Aiello, E., and M. Sleigh. 1977. Ciliary Function of Frog Oro-Pharyngeal Epithelium. Cell Tissue Res. 178:267-278.
7. Camalet, S., and F. Julicher. 2000. Generic aspects of axonemal beating. New Journal of Physics 2:1-23.